Active Integrated Antenna Technique

Tomohiro Seki†, Fusao Nuno, Kenjiro Nishikawa, and Keizo Cho

Abstract

We clarified the mounting precision for the active integrated array antenna for 25-GHz-band wireless access communication systems and confirmed that wirebonding is useful in constructing such antennas for the quasi-millimeter-wave frequency band, resulting in low-cost antenna systems. We also present an active integrated antenna configuration designed for broadband mobile wireless access systems using the 25-GHz band. The antenna and RF circuits are integrated into each side of a thick copper backing plate and they are connected through microstrip line/slot transitions. The antenna exhibited output power of 14.6 dBm and a noise figure of less than 5 dB. A wireless system using this antenna showed a 6-dB improvement in packet error rate compared with one using a passive antenna with the same array design. Furthermore, we obtained the first license for an active integrated antenna for high-speed wireless communication systems in Japan.

1. Introduction

System designs and wireless equipment for broadband mobile wireless access systems have been proposed and developed to achieve seamless communications [1]-[4]. A broadband mobile wireless access system with faster data transmission (over 100 Mbit/s) must use frequencies corresponding to quasi-millimeter or millimeter wave frequencies and have compact wireless terminals. This system must use a wider frequency band to achieve faster data transmission, while a compact terminal is desirable for mobile use. The use of high frequency also requires high output power due to the huge propagation loss and passive circuit losses. However, it is difficult to achieve high power in a compact wireless terminal. Active integrated array antenna technology that mounts the amplifier for transmitting and receiving without using a connector and a cable has been proposed and applied to broadband wireless access systems [5]-[8]. This antenna significantly suppresses the transmis-

sion loss between the antenna module and the radio frequency (RF) module [5]-[7], resulting in a big improvement in the packet error rate (PER) performance [9]. However, the present active integrated array antenna [9] employs phase shifters and attenuators to compensate for the mounting error of the active integrated antenna to improve the yield rate. Using this antenna results in expensive and large RF systems. The mounting error is caused by deviations in the devices, monolithic microwave integrated circuit (MMIC) mounting positions, and wirebonding. Flip-chip technology is useful for suppressing the mounting error, but it is still expensive. Therefore, it is necessary to clarify whether the conventional mounting method can be used to make an active integrated antenna for the quasi-millimeter-wave frequency band without any adjustment.

This paper first clarifies the mounting precision for an 8×8 active integrated array antenna with four subarrays that is used in 25-GHz-band fixed wireless access systems. Experimental results show that wirebonding is useful for making active integrated array antennas. Next, this paper presents an active integrated antenna configuration designed for actual wireless communication systems using the 25-GHz band. This

† NTT Network Innovation Laboratories
  Yokosuka-shi, 239-0847 Japan
  E-mail: seki.tomohiro@lab.ntt.co.jp

active integrated antenna comprises a microstrip antenna (MSA) array and RF front-end circuits using spatial power combining schemes for lower power consumption of the power amplifiers. Furthermore, the antenna and RF circuits are integrated into each side of a thick copper backing plate and are connected through microstrip line (MSL)/slot transitions. The developed active integrated antenna showed output power of 14.6 dBm and a noise figure of less than 5 dB. Wireless systems using this antenna achieved a 6-dB improvement in the PER compared with one using a passive antenna, which must use a connector to connect the amplifier, with the same array design as the active integrated antenna.

The rest of this paper is organized as follows. Section 2 clarifies that the precision of the wirebonding is adequate for mounting the active integrated antenna for 25 GHz. The proposed concept of the active integrated antenna structure employing a thick heat sink plate is described in section 3. The design of the MSL/slot transition, which is a key part for assembling this antenna, is presented in section 4. Section 5 describes the performance of a prototype antenna. Finally, section 6 discusses the effects of using the proposed antenna structure in an actual wireless system.

2. Mounting precision

2.1 Requirements

We selected an 8×8 array structure with a 0.5 λo (free-space wavelength array spacing) for conventional fixed communications in which the directive gain is approximately 17 dBi. The structure compris-
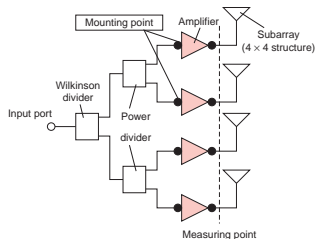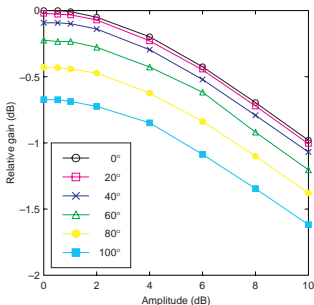
es four 4×4 sub-arrays. **Figure 1** shows a block diagram of the prototype. The mounting point for the Au wirebonding to connect the MMIC to the microstrip line is indicated in the figure. The calculated array antenna characteristics are given in **Fig. 2** when the feeding conditions between two sub-arrays were varied. Here, the amplitude and the phase represent the

(a) Gain reduction characteristics
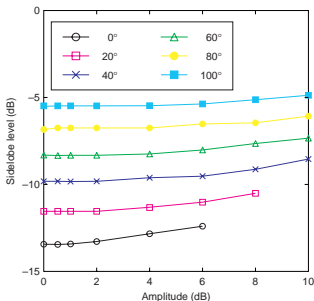
(b) Sidelobe level characteristics

Fig. 2. Calculated characteristics of active integrated antenna.

Fig. 1. Block diagram of test circuit for dispersion measurement.

difference in the feeding conditions between the two sub-array antennas. The moment method[*1] was used as the calculation method. **Figure 2(a)** shows the gain characteristics and **Fig. 2(b)** shows the sidelobe level characteristics. These figures suggest that variations in the gain and sidelobe levels occur due to slight differences in the feeding conditions. For example, when the variation in the feeding power is approximately 1.0 dB, the variation in the antenna gain is less
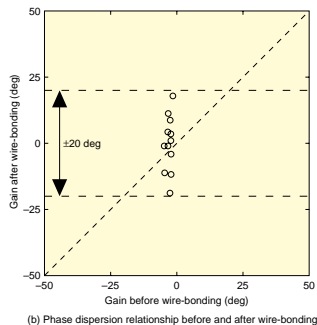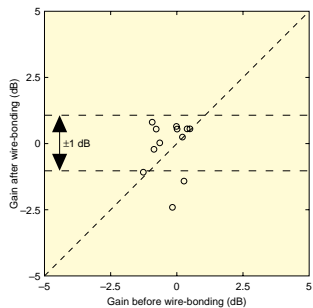
than 0.1 dB. Furthermore, the effect of the sidelobe level is small, while the effect of the feeding phase is large. Therefore, the mounting phase error must be less than 40° to achieve a sidelobe level of less than −10 dB.

2.2 Measurement results

(a) Mounting precision

To determine the mounting error, we constructed three active integrated antennas based on the same design. The measured mounting characteristics in the 25-GHz band using an MMIC chip (CHA2093, United Monolithic Semiconductors, Orsay, France) are shown in **Fig. 3**. Here, "before wirebonding" represents on-wafer measurements and "after wirebonding" represents the measured characteristics of the amplifier mounted on the antenna substrate. **Figure 3(a)** shows the gain dispersion characteristics before and after Au wirebonding, and **Fig. 3(b)** shows the phase dispersion characteristics before and after. In these figures, the measurement point is the mounting point indicated in Fig. 1. In Fig. 3, the dispersion of the gain is less than ±1 dB, and the dispersion of the phase is less than ±20°. These results clarify that the prototype antennas satisfy the necessary requirements.

(b) Total characteristics

The measured horizontal plane radiation pattern is shown in **Fig. 4**. We prepared three antennas to veri-

---

*1 A moment method is the most conventional electromagnetic method of analyzing the packaging of the high-frequency circuit and antennas. There is a lot of commercial software based on the moment method.

(a) Gain dispersion relationship before and after wire-bonding

(b) Phase dispersion relationship before and after wire-bonding

Fig. 3. Relationship between gain and phase dispersion before and after wire-bonding.
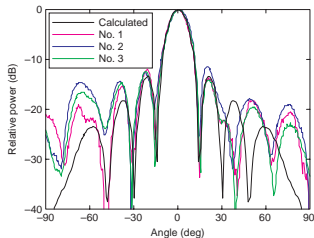

Fig. 4. Horizontal-plane radiation pattern of tested active integrated antennas.

fy the dispersion characteristics. The main lobe and sidelobe shapes agree with the calculated values and the radiation patterns of the three antennas are in good agreement, so we conclude that wirebonding achieves an adequate level of precision for the active integrated antenna at 25 GHz.

3. Design concept of active integrated antenna for broadband mobile wireless access systems

The design specifications required for this system are given in **Table 1**. **Figure 5** is a block diagram of the prototype active integrated antenna. The array antenna is divided into two sets of sub-arrays individually connected to each RF sub-circuit. In the transmission system, radiated powers from the sub-arrays are spatially combined to achieve the designed radiation characteristics and the total transmission power.

In order to eliminate the degradation caused by inefficient power combination, the power amplifiers must all have equivalent electrical properties. However, MMIC characteristics always vary individually,

and even if the same MMICs are used, their electrical properties will differ due to the conditions when they are mounted onto the substrates. Therefore, the circuits have voltage variable attenuators (VVAs) and phase shifters to adjust the amplitudes and phases of the two sub-arrays in the transmission system. However, there are no VVAs in the receiving system because their insertion loss is intrinsically large, and the noise figure is deteriorated by these attenuators.

4. Design of prototype active integrated antenna

4.1 Antenna structure

Figure 6 shows a cross-section of the prototype active integrated antenna for 25 GHz. The prototype has two sub-arrays constructed with 6×3 elements, giving it an adequate antenna-directivity margin of 17.0 dBi. Here, each antenna element is 3.64 mm × 3.64 mm, and the array spacing is 0.71 λ_0. We used a 40Ω microstrip line for the feeding circuit to establish the whole feeding circuit with more than a 0.1-mm linewidth to use the composite feeding circuit structure. Moreover, we used the −23 dB Chebysheff distribution[*2] to achieve low sidelobe characteristics. RF front-end circuits were etched on a single-layer Diclad880 substrate (εr = 2.17, 0.127 mm thick, ARLON Inc., Santa Ana, CA, USA). Each antenna array is etched on a two-layer structure comprising Diclad880 substrates (εr = 2.17, 0.254 mm thick). The copper plate binds the RF front-end substrate and the antenna substrate for heat sinking. The feed circuits are arranged in the inner layer for broadband characteristics of the MSA element with a narrow feed-line. We used the TGA1073G (TriQuint Semiconductor Inc., Texas, USA) as the power amplifier and TGA1319A-EPU (TriQuint Semiconductor Inc.,

Table 1. Specifications.

	Tx	Rx
Frequency bands	24.75 GHz – 25.25 GHz	
Total gain	Greater than 27 dBi	Greater than 31 dBi
Directivity gain	Greater than 17.0 dBi	
Output power	12.0 dBm – 15.8 dBm	—
Noise figure	—	Less than 7 dB
Spurious characteristics	Less than −26.0 dBm	—
Antenna size	75 mm × 75 mm	

*2 Chebysheff distribution is one of the most commonly employed distributions in filter design and is suitable for setting the sidelobe to less than a desired level.

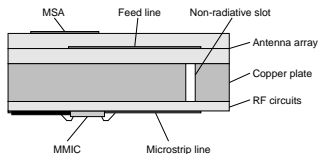SPDT: single-pole double throw

Fig. 5. Block diagram of active integrated antenna.

Fig. 6. Cross-sectional view of active integrated antenna.

Texas, USA) as the low noise amplifier. The copper backing plate is 69 mm × 75 mm × 3 mm in order to function sufficiently well as a power amplifier heat sink and to have sufficient mechanical strength. The non-radiating slot that penetrates the copper backing plate establishes a connection from one antenna array to the RF front-end circuits.

4.2 MSL/slot transition design

Figure 7 shows the structure of an MSL/slot transition. When the slot length L is approximately λ/2, the slot resonates. However, it is necessary to lengthen the slot to achieve sufficient matching and suppression of the loss of the MSL/slot transition as the metal thickness increases. Suppressing this power leak is also important to minimize the transmission loss. The input impedance is matched by adjusting stub lengths d1 and d2 and slot width W. **Figure 8** shows the relationship between the calculated minimum insertion loss of the MSL/slot transition and the metal thickness and the value of the slot length when the inser-
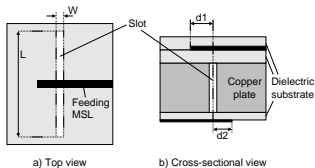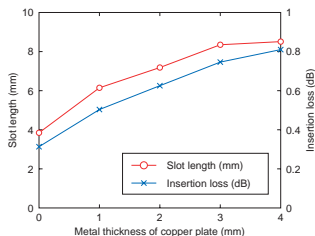
tion loss is minimum. Here, we use the finite element method in the simulation. The slot width is 0.5 mm determined by the minimum manufacturing process, and the stub lengths, d1 and d2, are optimized to minimize the loss of the MSL/slot transition. For metal thicknesses of 0, 1, 2, 3, and 4 mm, the optimized values of d1/d2 are 1.50/1.80, 1.20/1.50, 1.15/1.20, 1.50/1.65, and 1.60/1.65 mm, respectively. In Fig. 8, it is clear that the slot length is determined by the metal thickness, and the insertion loss increases linearly in proportion to it. We decided that the metal thickness should be 3 mm to provide adequate heat sinking and to accommodate the assembly.

5. Performance of prototype active integrated antenna

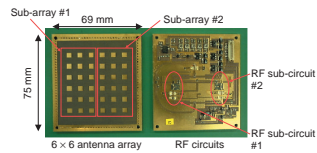The prototype active integrated antenna is shown in **Fig. 9(a)**. It is 75 mm × 69 mm. The transmission test system for it is shown in **Fig. 9(b)**.

Figures 10(a) and **10(b)** show the antenna's transmission (Tx) and reception (Rx) radiation patterns at 25 GHz, respectively. Here, the solid line represents results for the vertical plane and the dotted line represents those for the horizontal plane. These results show good performance for the spatial power combining mechanism.

Table 2 gives the measured and estimated total gains of the active integrated antenna at 25 GHz. For transmission and reception, they were 29.0 and 35.4 dBi, respectively. The measured gains were higher than the estimated values because the measured antenna directivity was approximately 1.5 dB higher than the estimated value.

Since it was difficult to measure the noise figure of the active integrated antenna, we measured the noise figure of the front-end circuit without the antenna or the MSL/slot transition. The measured noise figure was less than 3.4 dB. Accordingly, the total noise figure of the active integrated antenna is less than 5 dB because the loss of the MSL/slot transition and the MSL is approximately 1.6 dB.

To acquire a license for the experimental station of the 25-GHz band wireless communication system, we confirmed the characteristics of the manufactured active integrated antenna. The specifications under the license and the actual results for the active integrated antenna are given in **Table 3**. We also confirmed that the spurious characteristics, i.e., the undesirable frequency components, are less than –35.0 dBm outside the 25-GHz band. The transmission output power is 14.6 dBm at the output of the

Fig. 7. Structure of MSL/slot transition.

Fig. 8. MSL/slot transition characteristics versus metal thickness.

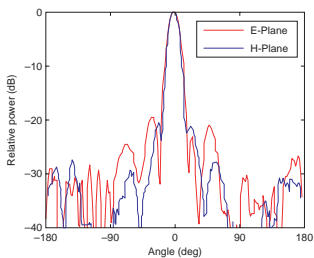(a) 6 × 6 antenna and RF front-end circuits of active integrated antenna

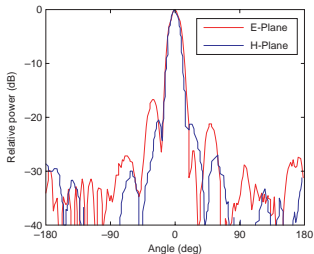(b) Transmission test system using active integrated antenna

Fig. 9. Photograph of prototype active integrated antenna and transmission test system.

(a) Tx radiation pattern at 25 GHz

(b) Rx radiation pattern at 25 GHz

Fig. 10. Radiation characteristics of prototype active integrated antenna.

Table 2. Measured and estimated total gains.

	Tx	Rx
Measured total gain (dBi)	29.0	35.4
Estimated total gain (dBi)	28.15	32.55
PA(Tx) and LNA(Rx) (dB)	22	19
Loss of RF front-end circuits (dB)	−10.85	−3.45
Directivity gain (dBi)	17	17

Table 3. License specifications of experimental station and measured results.

	Specifications	Measured resuts
Frequency deviation	Less than 7539 kHz	Less than 2 kHz
Output power	12.0 dBm − 15.8 dBm	14.6 dBm
Spurious characteristics	Less than −26 dBm	Less than −35 dBm
Occupied frequency bandwidth	Less than 18 MHz	Less than 16.5 MHz

time division duplexing (TDD) switch circuit connected to the sub-array antenna. These results show that this antenna satisfies the license specifications. Furthermore, we confirmed that this antenna has sufficient thermal stability because the fluctuation of its total gain over five hours was less than 0.5 dB.

6. PER improvement achieved using active integrated antenna

It is necessary to evaluate the effect of using the prototype active integrated antenna in practical wireless systems. Accordingly, we examined the improvement in PER characteristics using a transmission test system [4] that uses coded orthogonal frequency division multiplexing (OFDM) modulation based on the MMAC-HiSWANb specification. The measurements were performed in an anechoic chamber. The distance between the transmitting and receiving antennas was 3.0 m. A programmable attenuator was used to control the variation in transmission power. The PER characteristics for the prototype active integrated antenna and a passive antenna are given in **Fig. 11**. We used 16QAM with coding rate R = 9/16 for the modulation where the transmission rate was 27 Mbit/s. The passive antenna used the same antenna and feeding circuit design. Moreover, the outputs from the two sub-arrays were directly combined at the RFin & RFout terminals without any devices. The figure clearly shows that the PER results were approximately 6 dB better than for the passive
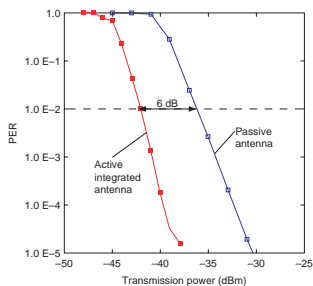
antenna when the PER value was 1.0×10^{-2}. Based on these results, we clarified that the noise figure of the active integrated antenna is less than 5 dB because the total noise figure of the transmission test system using a passive antenna is approximately 11 dB including the loss of the coaxial cable used to connect the transmission test system to the antenna terminal. Accordingly, we conclude that using the active integrated antenna is a very effective way of extending the transmission distance.

7. Conclusion

Since wirebonding, which is a typical method of mounting MMICs, is used to reduce the mounting cost, we investigated its mounting precision in the construction of active integrated antennas for the 25-GHz band. We constructed four spatial power-combining array antennas for the 25-GHz band mounted by wirebonding. The test results showed that the power dispersion and phase dispersion of the mounting precision were ±1 dB and ±20°, respectively. The results also showed that wirebonding is useful in constructing an active integrated antenna that forms a fixed narrow beam in the quasi-millimeter-wave frequency band.

We proposed an active integrated antenna configuration designed for broadband mobile wireless access systems using the 25-GHz band and made a prototype active integrated antenna, integrating a 6 × 6 antenna array and RF front-end circuits on each side of a thick copper backing plate for power amplifier heat sinking. The MSL/slot transition was designed taking into account non-radiating slots and exhibited good performance. The prototype antenna achieved adequate output characteristics when the power was 14.6 dBm and the noise figure was less than 5 dB. We examined the advantages of using the prototype active integrated antenna. The experimental results confirmed that the PER was improved by approximately 6 dB compared with a passive antenna using the same antenna design.

We also obtained the first license in Japan to use an active integrated antenna that does not have any measuring points between the antenna and the front-end circuit for high-speed wireless communication systems. We will verify the characteristics of the prototype active integrated antenna through field research.

Fig. 11. Measured PER versus transmission power of access point station (16QAM, R=9/16).

References

[1] Y. Takimoto, "Recent activities on millimeter wave indoor LAN sys-

tem development in Japan," in IEEE MTT-S Int. Symp. Dig., Orlando, U.S.A., pp. 405-408, Jun. 1995.

[2] N. Morinaga and A. Hashimoto, "Technical trend of multimedia mobile and broadband wireless access systems," Trans. IEICE., Vol. E82-B, No. 12, pp. 1897-1905, Dec. 1999.

[3] T. Ihara and K. Fujimura, "Research and development of millimeter-wave short-range application systems," Trans., IEICE, Vol. E79-B, No. 12, pp. 1741-1753, Dec. 1996.

[4] T. Atsugi, D. Uchida, M. Sugita, T. Seki, and M. Umehira., "A Transmission Test System using Quasi-millimeter Wave Band for Broadband Mobile Wireless Access System," Proc. of IEICE General Conf., Tokyo, Japan, B-5-156, Mar. 2002.

[5] M. P. Delisio and R. A. York, "Quasi-optical and spatial power combining," IEEE Trans. on MTT, Vol. 50, No. 3, pp. 929-936, Mar. 2002.

[6] K. Chang, R. A. York, P. S. Hall, and T. Itoh, "Active integrated antennas," IEEE Trans. on MTT, Vol. 50, No. 3, pp. 937-944, Mar. 2002.

[7] T. Seki, K. Uehara, and K. Kagoshima, "A Three-Dimensional Active Antenna for a High-Speed Wireless Communication Application," IEEE MTT-S Int. Microwave Symp., Denver, USA, Vol. 2, pp. 975-978, Jun. 1997.

[8] T. Hori and T. Seki, "New Multilayer Techniques Actualizing Active Antenna Hardware for Wireless Communication Systems," IEEE 11th Int. Conf. on Ant. and Prop., Manchester, United Kingdom, Vol. 2, pp. 479-483, Apr. 2001.

[9] T. Seki, F. Nuno, T. Atsugi, M. Umehira, J. Sato, and T. Enoki, "25 GHz Band Active Integrated Antenna for Broadband Mobile Wireless Access Systems," IEICE Trans. Electron., Vol. E86-C, No. 8, pp. 1520-1526, Aug. 2003.

Tomohiro Seki
Research Engineer, Wireless Systems Innovation Laboratory, NTT Network Innovation Laboratories.
He received the B.E. and M.E. degrees in electrical engineering from the Science University of Tokyo, Tokyo in 1991 and 1993, respectively. In 1993, he joined the NTT Radio Communication Systems Laboratories (now NTT Network Innovation Laboratories), Yokosuka, Japan. He has been engaged in the development of array antennas and active antennas for the millimeter-wave and microwave bands. He received the Young Engineer Award from the Institute of Electronics, Information and Communication Engineers (IEICE) Japan in 1999. He is a member of IEEE and IEICE.

Fusao Nuno
Research Engineer, Wireless Systems Innovation Laboratory, NTT Network Innovation Laboratories.
He received the B.E. degree in electrical engineering from Ehime University, Ehime in 1991 and the M.E. degree in electrical engineering from Kumamoto University, Kumamoto in 1993. In 1993, he joined the NTT Network Innovation Laboratories), Yokosuka, Japan. He has been engaged in R&D of portable terminals and base stations for broadband wireless access systems.

Kenjiro Nishikawa
Senior Research Engineer, Wireless Systems Innovation Laboratory, NTT Network Innovation Laboratories.
He received the B.E. and M.E. degrees in welding engineering from Osaka University, Suita, Osaka in 1989 and 1991, respectively. In 1991, he joined the NTT Radio Communication Systems Laboratories (now NTT Network Innovation Laboratories), Yokosuka, Japan. He has been engaged in R&D of three-dimensional and uniplanar MMICs on Si and GaAs and their applications. His current interests are millimeter-wave MMIC design/packaging technologies and microwave/millimeter-wave communication systems. He received the 1996 Young Engineer Award from IEICE. He is a member of IEEE and IEICE.

Keizo Cho
Director of Antenna and Propagation Group, Wireless Link Development Department, NTT DoCoMo.
He received the B.E. degree in electrical computer engineering from Yokohama National University, Yokohama in 1986, the M.E. degree in information processing from Tokyo Institute of Technology, Tokyo in 1988, and the Dr.Eng. degree in electrical engineering from Tokyo Institute of Technology, Tokyo in 2002. In 1988, he joined NTT Radio Communication Systems Laboratories (now NTT Network Innovation Laboratories), Yokosuka, Japan. He was a visiting researcher at the Communications Research Laboratory, McMaster University, Hamilton, Ontario, Canada from 1994 to 1995. He moved to the Wireless Link Development Department, NTT DoCoMo, Yokosuka, Japan in 2003. He has been engaged in R&D of base station and terminal antennas for mobile communication systems and advanced wireless communication systems. He received the Young Engineer Award from IEICE in 1995. He became Secretary of the IEICE Technical Group on Antennas and Propagation in 2003. He is a senior member of IEEE.